Simulation of Effect of Wind Barriers on Airflow

L. J. Hagen, E. L. Skidmore, P. L. Miller, J. E. Kipp
ASSOC. MEMBER
ASAE

ABSTRACT

LACK of a quantitative theory to explain airflow near wind barriers in the atmospheric boundary layer has hindered experimental programs in barrier research and made optimum barrier design for practical applications difficult. Our objectives were to develop a quantitative, theoretical simulation of airflow normal to narrow wind barriers of various porosities and, when possible, verify the results using experimental data.

To simulate the airflow near wind barriers, we used five linked, partial differential equations. The differential equations described the conservation of horizontal momentum, vertical momemtum, mass, turbulence energy, and dissipation rate of turbulence energy. Finally, we used an algebraic turbulence model to relate the turbulent viscosity to the turbulent energy and to the turbulent energy dissipation rate. We used finite difference methods having a combination of upwind and central difference schemes to solve the equations. As a barrier boundary condition, the porous wind barriers were treated as sources of horizontal velocity. The source strengths for 20-, 40-, and 60-percent-porous slat-fence barriers were determined by measuring the windspeed profiles at 0.5 to 1.0 barrier heights (H) leeward.

For experimental verification of the simulation model, windspeed reduction was measured leeward of 20-, 40-, and 60-percent-porous barriers having a ratio of H to a roughness parameter (z_o) of $H/z_o = 75$ and compared with the simulated results. Windspeed reduction data in the literature also were compared with simulated windspeed reduction with $H/z_o = 300$. Finally, vertical profiles of turbulence energy were measured near a 40-percent-porous wind barrier and compared with the simulated results.

Treating porous barriers as a source of horizontal velocity appears to be a valid method to obtain useful simulation results because the leeward simulated and measured windspeed patterns generally agreed well. The windspeed profiles measured at 0.5 to 1.0 H leeward of porous barriers can be used as a measure of the source strength; however, it was necessary to average several profiles to obtain an adequate estimate of source strength.

Article was submitted for publication in September 1980; reviewed and approved for publication by the Soil and Water Division of ASAE in January 1981. Presented as ASAE Paper No. 80-2034.

Contribution from U.S. Department of Agriculture, Science and Education Administration, Agricultural Research, in cooperation with the Kansas Agricultural Experiment Station. Dept. of Agronomy Contribution 80-346-A.

The authors are: L. J. HAGEN, Agricultural Engineer, and E. L. SKIDMORE, Soil Scientist, USDA-SEA-AR, Manhattan, KS; P. L. MILLER, Department Head, and J. E. KIPP, Professor, Mechanical Engineering Dept., Kansas State University, Manhattan.

INTRODUCTION

It is convenient to view changes produced by wind barriers in three stages. First, barriers change airflow in their vicinity. Second, the changed airflow pattern produces a microclimate and soil climate different from those in the open field. Finally, the altered microclimate and soil climate in the sheltered area produce a response in plants and livestock. Thus, predicting the airflow about barriers is a necessary first step toward complete quantification of barrier effects.

Several workers, particularly Tani (1958), Kaiser (1959), and Counihan et al. (1974), have described theoretically certain aspects of the problem, but the ability of their methods to predict airflow about barriers is quite limited. The objectives of this investigation were to develop a quantitative, theoretical simulation of airflow normal to narrow wind barriers of various porosities and, when possible, to compare the results with experimental data.

Reviews of the aerodynamics of wind barriers by Plate (1971) and Raine and Stevenson (1977) showed that the airflow patterns about wind barriers are complicated. In the simplest case of a long barrier normal to the flow, the flow is two-dimensional, incompressible, and in practical cases, turbulent. Among the barrier properties that affect the flow are barrier width, shape, and resiliency, with barrier height and porosity the major properties.

Flow about barriers is further complicated because barriers are placed in the earth's boundary layer. Barriers are usually within the so-called "constant-stress region" near the surface where the open-field windvelocity profile is described by

$$\frac{u}{u_*} = \frac{1}{k} \ln\left(\frac{z - d}{z_o}\right) + f(Ri) \quad \ldots\ldots\ldots\ldots\ldots\ldots\ldots\ldots \quad [1]$$

where u is mean velocity, u* is friction velocity, z is height of measurement from some reference plane, d is zero-plane displacement height, z_o is a roughness parameter, and k is von Karman's constant ($\cong 0.4$). The last term on the right of equation [1], f(Ri), indicates that mean velocity also depends on Richardson's number (Ri), which is a measure of atmospheric stability. Under neutral stability this term is near zero.

From equation [1] it is obvious that both surface roughness and stability of the air influence airflow about barriers. In an atmospheric boundary layer with neutral stability, the airflow patterns near two geometrically similar barriers (a and b) will be similar provided $(H/z_o)_a = (H/z_o)_b$, where H is barrier height.

METHODS AND PROCEDURES

The partial differential equations that describe the airflow normal to a wind barrier in the earth's boundary

layer were developed. A suitable turbulence model was selected to provide closure for the equations, then finite difference methods were used to solve the equations. Outdoor field experiments were used to supply some of the boundary conditions for the theoretical calculations as well as to verify some of the calculated results.

THEORETICAL

Differential equations

Flow normal to a barrier is two-dimensional and can be described by the Navier-Stokes equations for conservation of momentum. For incompressible, steady, two-dimensional flow, the momentum equations in Cartesian coordinates become

$$\rho(u\partial u/\partial x + w\partial u/\partial z) = -\partial p/\partial x + 2\partial/\partial x(\mu\partial u/\partial x) + \partial/\partial z(\mu\partial u/\partial z) + \partial/\partial z(\mu\partial w/\partial x) \quad [2]$$

and

$$\rho(u\partial w/\partial x + w\partial w/\partial z) = -\partial p/\partial z + 2\partial/\partial z(\mu\partial w/\partial z) + \partial/\partial x(\mu\partial u/\partial z) + \partial/\partial x(\mu\partial w/\partial x) \quad [3]$$

where u is horizontal velocity in the x-direction, w is vertical velocity in the z-direction, μ is fluid viscosity, p is pressure, and ρ is fluid density. For the low velocities encountered in the atmospheric boundary layer, ρ was considered a constant.

Because there are three independent variables, u, w, and p, it is necessary to include the equation of continuity to complete the set of equations. For incompressible flow, it has the form

$$\partial u/\partial x + \partial w/\partial z = 0 \quad [4]$$

The three preceding equations completely specify a laminar wind barrier flow. Unfortunately, the atmospheric boundary layer is generally turbulent. To handle a turbulent flow, the variables u, w, and p must be considered properties of the mean flow and μ must be an effective (eddy) viscosity (μ_t) for the turbulent flow. The turbulence model selected to calculate μ_t has the form

$$\mu_t = \rho C_\mu K^2/\epsilon \quad [5]$$

where C_μ is a constant, K is turbulence energy, and ϵ is turbulence energy dissipation rate.

Both K and ϵ must be determined in the turbulence model. Launder and Spalding (1972) note that an exact equation for K can be derived from the Navier—Stokes equations. The procedure consists of multiplying the momentum equation for each coordinate direction by its cooresponding fluctuating velocity. Next, time averaging and summing the three equations gives a single equation with k as the independent variable. Finally, after some minor assumptions, the result is

$$\rho(u\partial K/\partial x + w\partial K\,\partial z) = \partial/\partial x(T_k\partial K/\partial x) + \partial/\partial z(T_k\partial K/\partial z) + S_k \quad [6]$$

where T_k is the effective exchange coefficient for turbulent energy computed from $T_k = \mu_t/\sigma_k$. The quantity σ_k is often called a turbulent Prandtl numer for diffusion of turbulent energy.

The source term, S_k, accounts for the creation and destruction of turbulent energy and has the form

$$S_k = 2\mu_t[(\partial u/\partial x)^2 + (\partial w/\partial z)^2] + \mu_t(\partial u/\partial z + \partial w/\partial x)^2 - \rho\epsilon \quad [7]$$

where

$$\rho\epsilon = \mu_t[\overline{(\partial u'/\partial x)^2} + \overline{(\partial u'/\partial z)^2} + \overline{(\partial w'/\partial x)^2} + \overline{(\partial w'/\partial z)^2}] \quad [8]$$

The primes denote instantaneous values.

The momentum equations also can be manipulated to derive an approximate equation for the dissipation term, ϵ, in the form

$$\rho(u\partial\epsilon/\partial x + w\partial\epsilon/\partial z) = \partial/\partial x(T_\epsilon\partial\epsilon/\partial x) + \partial/\partial z(T_\epsilon\partial\epsilon/\partial z) + S_\epsilon \quad [9]$$

where the source term S_ϵ is

$$S_\epsilon = C_1(\epsilon/K)\mu_t[(\partial u/\partial z + \partial w/\partial x)^2 + 2\{(\partial u/\partial x)^2 + (\partial u/\partial x)^2\}] - \rho C_2\epsilon^2/K \quad [10]$$

The effective exchange coefficient for turbulent dissipation rate, ϵ, is computed from $T_\epsilon = \mu_t/\sigma_\epsilon$ where σ_ϵ is a constant. The procedures and approximations used to derive the K and ϵ equations are shown by Hagen (1980).

Equations [2] through [10] form a set of linked equations. Only the boundary conditions and the constants remain to be specified. Finite difference methods were used to sequentially solve the partial differential equations.

Boundary Conditions and Constants

We made the boundary conditions and the differential equations dimensionless by using friction velocity, barrier height (H), and air density as scale factors. The domain over which the equations were solved and the boundaries are shown in Fig. 1. Locations of the side and top boundaries were selected to avoid barrier influence. Thus, the side and top boundary conditions remained constant for a given surface roughness.

The upwind side and top boundary conditions were as follows:

$$u/u_* = (1/k)\ln(z/z_o) \quad [11]$$

$$w = 0 \quad [12]$$

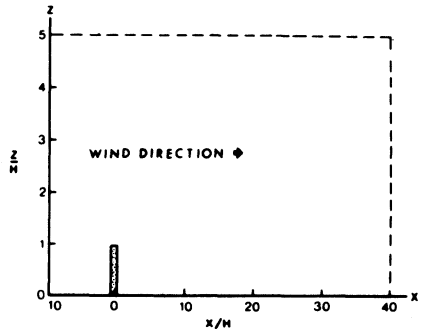

FIG. 1 Location of wind barrier and solution domain boundaries in multiples of barrier height (H) in vertical (z) and horizontal (x) directions.

$$p = 0 \quad \ldots\ldots [13]$$

$$K/u_*^2 = 1.0/C_\mu^{0.5} \quad \ldots\ldots [14]$$

$$\epsilon/u_*^3 = 1.0/(kz) \quad \ldots\ldots [15]$$

At the downstream, side boundary, the gradient of u was set equal to zero, while w, K, p, and ε were given the same values as at the upstream side boundary.

Steep gradients tend to increase inaccuracies in the finite difference solutions near the surface unless some modifications (wall functions) are applied to the equations. Launder and Spalding (1974) discussed the need for wall functions and developed some for smooth surfaces. Here, some approximate wall functions were developed for atmospheric flow and then substituted into the differential equations.

In the u-momentum equation, the term

$$(\mu_t \partial u/\partial z - \rho wu)|_s \quad \ldots\ldots [16]$$

was approximated as

$$(\mu_t \partial u/\partial z)|_s = \tau_s \frac{u_p}{u_p} \cong \frac{\rho C_\mu^{1/4} K_p^{1/2}}{(1/k)\ln(z_p/z_o)} u_p \quad \ldots\ldots [17]$$

where P is the grid point nearest the surface s, and τ_s is surface shearing stress.

In the w-momentum equation, the term

$$(\mu_t \partial w/\partial z - \rho ww)|_s \quad \ldots\ldots [18]$$

was set equal to zero, which implies no diffusion of w-momentum to the surface.

In the K-equation, the approximation

$$[\iint \mu_t (\partial u/\partial z + \partial w/\partial x)^2 dzdx]|_p \cong \tau_s (\partial u/\partial z)|_p \Delta x \Delta z$$

$$\cong \frac{\tau_s u_p \Delta x \Delta z}{z_p \ln(z_p/z_o)} \quad \ldots\ldots [19]$$

was used where τ_s was calculated in equation [17]. The approximation

$$(T_K \partial K/\partial z - \rho wK)|_s \cong 0 \quad \ldots\ldots [20]$$

also was used, and it implies no diffusion of K to the surface. The final approximation used in the K-equation was

$$\frac{C_\mu \rho^2 K_p \Delta x \Delta z}{\mu_t}\Big|_p \cong \frac{\rho C_\mu^{3/4} K_\rho^{1/2} \Delta x \Delta z}{kz_p} \quad \ldots\ldots [21]$$

The rates of creation and destruction of turbulent energy at point P near the surface were assumed to be in equilibrium. Consequently, ϵ_p was calculated as

$$\epsilon_p = \frac{C_\mu^{3/4} K_p^{3/2}}{kz_p}. \quad \ldots\ldots [22]$$

Shir (1972) also imposed equation [22] as a boundary condition in modeling flow at a change of surface roughness.

Boundary conditions at solid, artificial barriers can be treated like those at the surface. For porous barriers, however, little is known about the boundary conditions. Consequently, the boundary condition was chosen to minimize the necessary inputs. A displaced grid system (Harlow and Welch, 1965) was employed in which the scalar variables were calculated at the grid nodes, and the velocity variables were calculated at the internode positions. The barrier was placed at the internode position and treated as a source of horizontal velocity.

The constants used in the differential equations were taken from the literature and from experimental data of this investigation. In the open field $C_\mu = u^{*4}/K^2$ and was measured as ≅ 0.026. The derivations of C_1 and C_2 are discussed by Launder and Spalding (1972). After using a computer to optimize the constants in various turbulent flows, Gosman et al. (1977) recommended $C_1 = 1.44$, $C_2 = 1.92$, $\sigma_K = 0.9$, and $\sigma_\epsilon = 1.22$. These values were used in the present work.

EXPERIMENTAL

All the experimental work was done on a 90- × 150-m, level field with its longest dimension oriented north-south. The field was covered with a mixture of grasses and weeds, which were mowed periodically to maintain a uniform surface (z_o = 0.5 to 2.0 cm). There were no nearby, upwind obstructions, but various crops were grown on adjacent, upwind fields. Slat-fences of various porosities were erected somewhat north of the field center in an east-west direction because the prevailing wind direction was southerly. Slat-fence barriers 1.22 and 2.44 m tall were used in various parts of the experiment. The tall barrier was 80 m long and the short barrier, 50 m. Slat widths ranged from 3 to 4 cm in all barriers.

The experimental work was accomplished in three parts, and Table 1 summarizes the measurements obtained. During all parts of the experiment, windward profiles of windspeed and temperature as well as wind direction were monitored in the open field. The windward data were used to monitor atmospheric stability to ensure that it was near neutral or only slightly unstable

TABLE 1. SUMMARY OF MEASUREMENTS OBTAINED IN EACH PART OF WIND BARRIER EXPERIMENTS

Part of experiment	Measured variables	Transducers	Position relative to wind barrier
All parts	Windspeed profile	Cup anemometers	Windward
	Wind direction	Vane	Windward
	Temperature profile	Thermocouples	Windward
Airflow through barriers	Windspeed profile	Cup anemometers	Leeward
Windspeed reduction	Windspeed	Cup anemometer	Leeward
Turbulence energy	Vector wind velocities	UVW-anemometer	Windward
			Leeward

during data collection periods. Mean wind direction also was measured to ensure that it was normal to the barrier ± 15 deg. Finally, the windward windspeed profiles were used to calculate the displacement height (d) and surface roughness (z_o).

The windward windspeeds were measured simultaneously by cup anemometers at 32, 64, 100, 140, 190, and 250 cm above the surface. Naturally ventilated, radiation-shielded thermocouples were mounted in corks to given them a time constant of about 20 s. They were placed at 32, 64, 140, and 250 cm above the surface and used to measure the temperature difference between each level as well as absolute temperature at highest and lowest levels. The wind direction vane was mounted at a height of 250 cm.

A computer-controlled data acquisition system (DAS) monitored the transducers and printed averages and standard deviations of the data at the end of each 10-min period. The windspeed was continually recorded on pulse counters in the DAS. The thermocouples and wind direction vane were sampled for a 0.1-s period in each 2 s.

Airflow through barriers

One of the boundary conditions needed in the theoretical calculations for porous barriers is horizontal windspeed through the barrier. To measure it, one needs to measure close enough to the leeward side to avoid downstream changes induced by flow over the top, but far enough from the barrier to avoid laterally nonuniform flow caused by air jetting between the slats. After some preliminary trials, we used flow profiles at 0.5 to 1.0 H leeward of the barriers.

Airflow through slat-fence barriers 1.22 m tall and 20, 40, and 60 percent porous was measured. We added slats to commercial "snowfence" to achieve the various porosities. The upwind windspeed profile was measured as previously detailed, and five cup anemometers were used to measure the leeward profile. The cup anemometers were mounted at 15, 30, 60, 90, and 120 cm above the surface for one set of measurements, then moved to 20, 40, 60, 80, and 100 cm where the measurements were repeated.

Airflow also was measured through the 2.44-m-tall, 40-percent-porous barrier with leeward anemometers mounted at the same height as the windward ones.

Windspeed reduction

A cup anemometer was placed at z/H = 0.25 (≅ 30 cm) to measure leeward windspeed reduction near the surface. Two data runs each were made at positions 2, 4, 6, 9, and 12 H leeward of the 1.22-m-tall, slat-fence barriers.

Turbulence energy

A UVW-anemometer* mounted on a portable tower was used to measure profiles of turbulence energy near the 40-percent-porous, 2.44-m-tall barrier. The UVW-anemometer tends to underestimate the turbulent energy components, particularly the $\overline{w'^2}$ component, near the surface (Horst, 1973), so the 1.22-m-tall barriers were not used in this part of the experiment.

*Gill UVW-anemometer, Model 27002, R. M. Young Co. Mention of a product is for information only and does not constitute an endorsement by the U.S. Department of Agriculture, Science and Education Administration.

The UVW-anemometer consisted of three propeller anemometers with each propeller driving a d.c. tachometer generator. The 23-cm diameter propellers were mounted on 40-cm-long arms in an orthogonal array. Two arms (U and V) were mounted to bisect the horizontal wind, while the third was leveled in the vertical position. The windspeed signal from each propeller was recorded on separate channels of an analog, magnetic tape recorder at 45 or 75 cm/s tape speed. Calibration signals were also recorded on each channel, and a square wave was recorded on a separate channel.

For data analysis the UVW-data were played back at a tapespeed of 8.75 cm/s, and the channels serially sampled by the data acquisition system for 0.1 s each. Each sampling sequence was initiated by the square waves. The sampled data from each channel were averaged to form real-time averages of 0.125 s duration. An iterative computer algorithm described by Horst (1972) was used to correct the raw data for noncosine propeller response to give three simultaneous values, Gu, Gv, and Gw. Gu and Gv represented instantaneous components of the horizontal wind vector and Gw the instantaneous vertical wind vector. Mean flow velocities (u, v, w) and direction were then calculated.

After calculating mean flow velocites and direction, the data were again sampled by the data acquisition system, and the turbulent flow variables were computed and summed to given the turbulence energy (K) defined as

$$K = \frac{1}{2}(\overline{u'^2} + \overline{v'^2} + \overline{w'^2}). \quad \ldots\ldots\ldots\ldots\ldots\ldots\ldots\ldots [23]$$

The primes denote fluctuations from the mean velocities, and the overbar denotes an average.

RESULTS AND DISCUSSION

To simulate barrier performance in the theoretical equations, one must supply boundary conditions at the barrier. While it is easy to suggest many boundary conditions that should be supplied for the theoretical equations, in practice they have not been measured at most barrier surfaces. In addition, if one is forced to measure all of the boundary conditions at wind barriers, then the advantage of simulating the flow near barriers instead of relying on measurements is diminished. Thus, the approach we used was to treat the barrier as a source of fixed horizontal velocity. In the following sections we examined the utility of this procedure by comparing simulated results with experimental measurements.

The windspeed profiles used to represent the various barrier porosities in the simulation results are shown in Fig. 2. Each data point is an average of 2 to 5 observations measured at various lateral locations about 0.5 to 1.0 H leeward of the barriers. Obviously, there was some scatter in the data. The dynamic pressure on the upwind side of the barrier caused local jets when the slat distribution was not uniform. Thus, to establish representative profiles, windspeeds at several lateral locations were sampled. Windspeeds at the tops of the barriers were probably less than measurements indicated because this is a highly turbulent zone in which cup anemometers tend to overspeed. No attempt to correct the data was made, however.

The calculated, open-field, windspeed-profile parameters were averaged for all data runs. The average

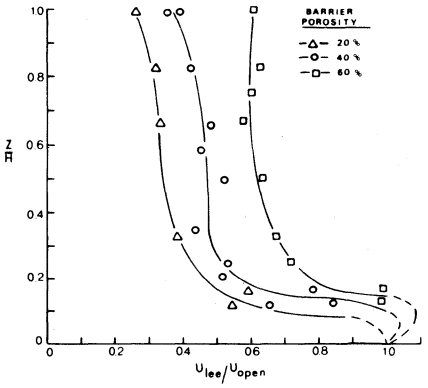

FIG. 2 Dimensionless windspeed profiles (u_{lee}/u_{open}) measured at 0.5 to 1.0 H leeward of various porosity barriers. Dashed lines indicate estimated windspeeds near the ground surface.

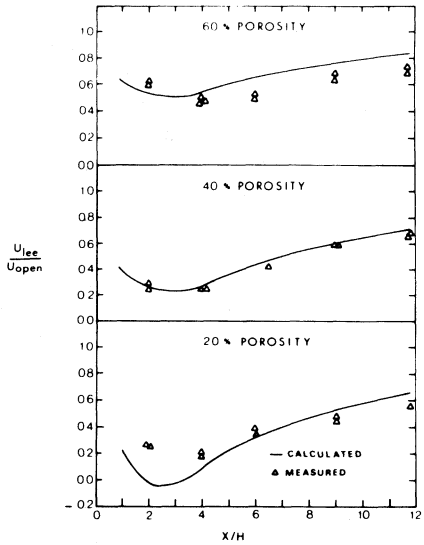

FIG. 3 Comparison of computed and measured windspeeds at a height of z/H = 0.25 leeward of 1.22-m-tall barriers.

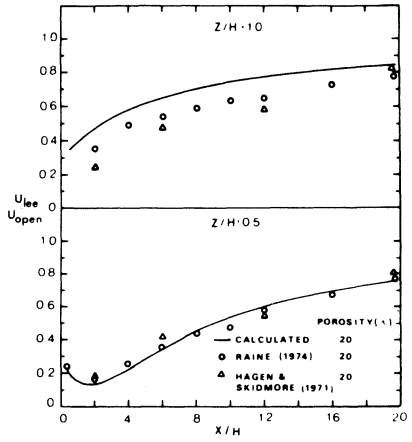

FIG. 4 Comparison of measured and computed windspeeds leeward of 20-percent-porous barriers.

z_o was 1.6 cm, and d was 5.0 cm during the windspeed reduction measurements near the short barriers. During measurements of turbulence energy near the tall barrier, z_o averaged 0.9 cm and d was 3.8 cm. The experimental tests were made during October with windspeeds of 4.5 to 10 m/s at 1.4 m height. Calculated values of Ri indicated atmospheric stability remained near neutral during all the tests.

Leeward Windspeed Reduction

Windspeeds near the 20-, 40-, and 60-percent-porous slat-fence barriers were computed and compared with measured windspeeds (Fig. 3). The barriers were 122 cm tall; thus, the H/z_o ratio for these tests was about 75. Measured and computed results generally agreed well, but the computed windspeeds were higher than the measured results leeward of the 60-percent-porous barrier except at 2 H. Evidently, the windspeeds in the profile used for the boundary condition on the 60-percent-porous barrier were slightly high.

A large deviation between computed and measured windspeed also appeared at 2 H leeward of the 20-percent-porous barrier. The computed results showed a small recirculation zone in that region with the top of the reversed flow layer reaching z/H = 0.25. Thus, high turbulence imposed on the low mean wind velocity caused the cup anemometer at 2 H to record windspeeds higher than actual.

Because changing H/z_o affects the leeward flow, the simulation model needed to be tested under additional conditions. Two sets of experimental data in the literature were chosen for additional testing of the simulation model. The first set was obtained near 2.44-m-tall slat-fence barriers by Hagen and Skidmore (1971) with porosities and field conditions similar to those used in the present work. The H/z_o ratio was 275.

A second set of data obtained from wind tunnel tests was recently reported by Raine (1974). He estimated that his H/z_o ratio was somewhat greater than that of Hagen and Skidmore. In the wind tunnel tests, the atmospheric boundary-layer windspeed profile was carefully simulated, and barriers with 20, 34, and 50 percent porosity were tested.

To simulate these data sets, an H/z_o ration of 300 was used to calculate u_{lee}/u^* profiles at the barrier. The results of the simulation and experiments are shown in Figs. 4, 5, and 6. Computed and measured windspeeds at $z_o/H = 0.5$ agreed well, but the simulated values at $z/H = 1.0$ were generally larger than measured. The latter result indicates that windspeeds at the top of the barriers used as a boundary condition were somewhat high. Additional measurements slightly below the barrier top should have been made to avoid the intensely turbulent region at the top.

The increased H/z_o ratio also reduced the recirculation zone leeward of the 20-percent-porous barrier, and the position z/H = 0.5 was above the center of the recirculation zone. In this case the experimental data and the simulated flow computations at 2 H agreed. This observation indicated the capacity of the simulation model to predict actual flow conditions. It also helped to explain the wide range of windspeed reductions in the literature for a given porosity. Evidently, both the H/z_o ratio and measurement height strongly influence the measured windspeed reduction.

The difference between wind tunnel and field data was particularly large near the 40-percent-porous barrier at

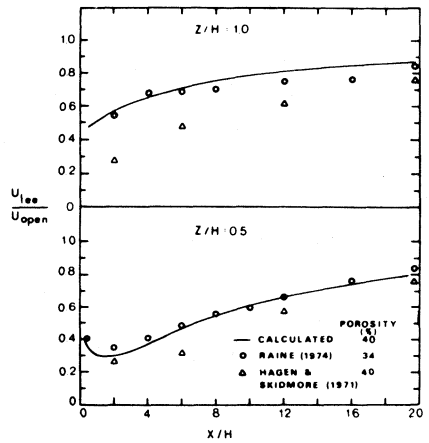

FIG. 5 Comparison of measured and computed windspeeds leeward of 34- and 40-percent-porous barriers.

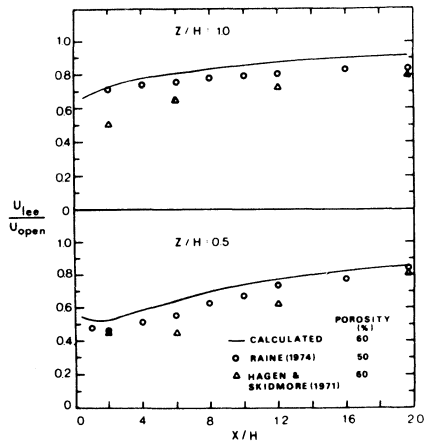

FIG. 6 Comparison of measured and computed windspeeds leeward of 50- and 60-percent-porous barriers.

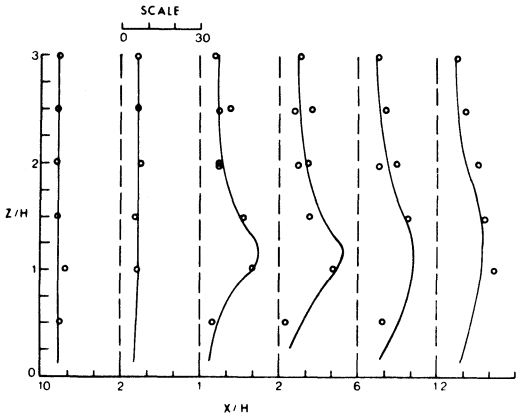

FIG. 7 Comparison of measured (circles) and computed (solid lines) turbulent energy (K/u^{*2}) near a 2.44-m-tall, 40-percent-porous, slat-fence barrier.

z/H = 1 (Fig. 5). Moderately unstable atmospheric conditions during this sequence of field measurements appear to have caused the difference. Close to the surface, instability effects are reduced and behave differently than at z/H = 1. Based on measurements at z/H = 0.25, Seginer (1975) reported atmospheric instability increased windspeeds near 10 H lee, but had little effect near 2 H where turbulence predominated.

Turbulence Energy

Turbulence energy (K/u^{*2}) measured in the open field was nearly constant with height and averaged 6.2 (Fig. 7). A value of 5.8 for turbulence energy from field data was reported by Fichtl (1973), whereas Shir (1972) used a turbulence energy of 4.6 to simulate shearing stress near a change-of-surface roughness. However, the maximum surface z_o was 0.25 cm in the data Shir was simulating, while our open field z_o averaged 0.9 cm during the turbulence measurements. In near-neutral atmospheric conditions, turbulence energy likely depends on surface roughness alone, but more experimental data are needed to determine the complete relationship.

The windward turbulence energy was used as a boundary condition, and H/z_o set equal to 300 in the simulation model to calculate turbulence energy profiles near the 40-percent-porous barrier (Fig. 7). A zone of maximum turbulence was created by a large wind shear near the top of the barrier. The computed and measured turbulence energies agreed well near the maximum turbulence zone.

At z/H = 0.5, the leeward turbulence energy measurements were less than predicted. Slow response by the UVW-anemometer caused a 10 to 20 percent reduction in measured turbulence energy near the surface (Horst, 1973). However, the remaining difference was probably caused by the simulation model indicating a more rapid diffusion of turbulence energy toward the surface than actually occurred.

Profiles of turbulence energy also are shown for 20-and 60-percent-porous barriers with H/z_o = 300 (Fig. 8). The calculated turbulence energy was lowest near the lee side of the 20-percent-porous barrier, which agrees with the behavior of turbulence intensity distribution measured by Raine and Stevenson (1977) near model fences in the wind-tunnel. Near z/H = 1, there was a large difference between the wind shear generated by the 20- and 60-percent-porous barriers. Maximum turbulence energies of 28, 23, and 16 were calculated for the 20-, 40-, and 60-percent-porous barriers, respectively. For barriers with the same porosities but with H/z_o = 75, calculated maximum turbulence energies were 19, 16, and 12.

CONCLUSIONS

The experimental measurements and computer simulations of airflow about porous barriers undertaken in this investigation support the following conclusions.

Treating porous barriers as a source of horizontal velocity greatly reduces the number of barrier boundary conditions; yet to a distance of 20 H leeward, the measured velocity distribution patterns were closely approximated by the computer simulation model. Thus, this approach appears to be a valid method for obtaining useful simulation results.

The windspeed profile measured at 0.5 to 1.0 H leeward of porous barriers with nearly uniform lateral porosity distribution can be used as a measure of the source strength to provide the boundary condition for the simulation model. However, at least three to five profiles at various lateral positions should be averaged to obtain an adequate estimate of the source strength.

At H/z_o = 300, predicted maximum turbulence energies (K/u^{*2}) were 15, 23, and 28 for the 60-, 40-, and 20-percent-porous barriers, respectively. The measured and predicted maximum energies agreed well near the

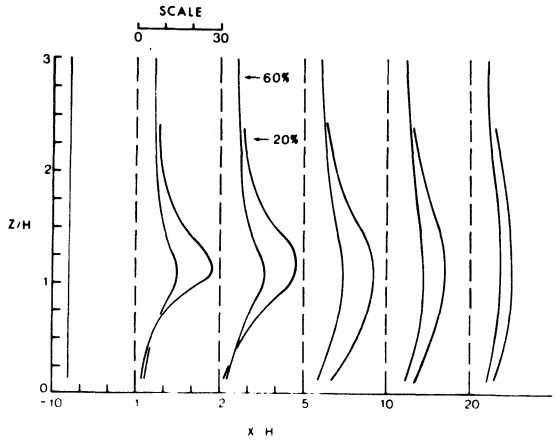

FIG. 8 Computed turbulence energy profiles (K/u^{*2}) for 20- and 60-percent-porous barriers.

40-percent-porous barrier, but the simulated rate of diffusion of turbulent energy to the surface was larger than measured. Further measurements with fast-response transducers are needed to quantify this difference. Decreasing H/z_o decreased the predicted maximum turbulence energy.

The simulation model is able to accurately predict even the most complex flow patterns near porous barriers such as the recirculation zone induced near the surface by the 20-percent-porous barrier. The simulation model also predicted that the recirculation zone size decreased as H/z_o increased.

References

1 Counihan, J., J. C. R. Hunt and P. S. Jackson. 1974. Wakes behind two-dimensional surface obstacles in turbulent boundary layers. J. Fluid Mech. 64(3):529-563.

2 Fichtl, G. H. 1973. Problems in the simulation of atmospheric boundary layer flows. AGARD Conf. Proc. No. 140.

3 Gosman, A. D., E. E. Khalil and J. H. Whitelaw. 1977. The calculation of turbulent recirculating flows. Symposium on Turbulent Shear Flows, Penn. State Univ., University Park, PA, pp. 13.35-13.45.

4 Hagen, L. J. 1980. Simulation of effect of wind barriers on airflow. Unpublished Ph.D. Dissertation, Kansas State Univ., Manhattan, KS.

5 Hagen, L. J. and E. L. Skidmore. 1971. Turbulent velocity fluctuations and vertical flow as affected by windbreak porosity. TRANSACTIONS of the ASAE 14(4):634-637.

6 Harlow, F. H. and J. E. Welch. 1965. Numerical calculation of time-dependent viscous incompressible flow of fluid with free surface. Physics of Fluids 8(12):2182-2189.

7 Horst, T. W. 1972. A computer algorithm for correcting non-cosine response in the Gill anemometer. PNL Annual Report for 1971 to USAEC Div. of Bio. and Medicine, Vol. II, BNWL-1651-1, Pacific Northwest Laboratories, Richland, WA.

8 Horst, T. W. 1973. Corrections for response errors in a three-component propeller anemometer. J. Appl. Meteorol. 12(5):716-725.

9 Kaiser, H. 1959. The wind-flow at shelterbelts. Translated by J. T. Godfrey, Bev. Dent. Wetterdienstes 7(53):1-36.

10 Launder, B. E. and D. B. Spalding. 1972. Mathematical models of tubulence. Academic Press, NY.

11 Launder, B. E. and D. B. Spalding. 1974. The numerical computation of turbulent flows. Computer methods in Appl. Mech. and Engr. 3:269-289.

12 Plate, E. J. 1971. The aerodynamics of shelterbelts. Agr. Meteorol. 8(3):203-222.

13 Raine, J. K. 1974. Wind protection by model fences in a simulated atmospheric boundary layer. Fifth Australasian Conf. on Hydraulics and Fluid Mech., Univ. of Canterbury, Christchurch, New Zealand, pp. 200-210.

14 Raine, J. K. and D. C. Stevenson. 1977. Wind protection by model fences in simulated atmospheric boundary layer. J. Industrial Aero. 2:159-180.

15 Seginer, I. 1975. Atmospheric stability effect on windbreak shelter and drag. Boundary Layer Meteorol. 8:383-400.

16 Shir, C. C. 1972. A numberical computation of airflow over a sudden change of surface roughness. J. Atmos. Sci. 29(2):304-310.

17 Tani, N. 1958. On the wind tunnel test of the model shelter hedge. (In Japanese with English summary.) Bull. Nat. Inst. Agr. Sci. A., No. 6.